GSA Data Repository Item 2016102
Turnbull, R., Tulloch, A., Ramezani, J., and Jongens, R., 2016, Extension-facilitated pulsed S-I-A-type "flare-up" magmatism at 370 Ma along the southeast Gondwana margin in New Zealand: Insights from U-Pb geochronology and geochemistry: GSA Bulletin, doi:10.1130/B31426.1.

Tables S1 and S1

Supplementary Online Material

S1. U-PB ANALYTICAL METHODOLOGY

In situ U-Pb zircon geochronology and trace element analysis (LA-ICPMS)

Clean rock crushing and high-density mineral separation followed by magnetic extraction of zircon was undertaken at GNS Science. Approximately 50 grains from each sample were hand-picked under binocular scope and mounted in epoxy. Emphasis was placed on selecting a wide variety of zircon sizes, morphologies and internal structures in order to minimize sampling bias. Before analysis, all grains were imaged with reflected and transmitted light to identify cracks and mineral and melt inclusions, and thus guide analysis locations. Au-coated zircon mounts were then imaged by cathodoluminesence (CL) in a Hitachi S360 SEM g at the Research School of Earth Sciences (RSES), Australian National University, to aid in identification of recrystallization textures and inherited cores (Fig. 3). On the basis of zircon images, 40–45 grains were selected for analysis by LA-ICPMS at the RSES, following procedures reported by Ballard et al., (2001). Details of operating conditions are outlined below.

Laser ablation utilized a pulsed LambdaPhysik LPX 120I UV ArF excimer laser operated at a constant energy of 23kv, using a spot diameter of 32 μm. Ablated material was carried by a mixed He-Ar gas from a custom-designed sample cell and flow homogenizer to an Agilent 7500 ICP-MS. Zircon rims and tips were specifically targeted in order to determine magmatic crystallization ages, and core and mid sections were also targeted to assess zircon inheritance. Data were referenced to the zircon standard TEMORA 2 (TEM2) (Black et al. 2004) and NIST SRM 610 glass, which were both analyzed once for every 10 unknowns. Background data was acquired for ~20sec followed by ~40sec of laser ablation, yielding around 100 mass scans and an estimated penetration depth of 20μm. Processing of raw data was achieved offline with a series of excel workbooks. Instrumental drift and penetration depth fractionation were corrected via reference to data collected for the standards averaged for each analytical session. All hand specimens, thin sections, mineral separates and sample mounts are stored within the GNS Science PETLAB database collection (http://pet.gns.cri.nz). The zircon standard R33 was also measured as an unknown during analyses, and was calibrated against the TEMORA2 standard to assess accuracy of results. The weighted mean dates calculated from the two sessions (18/05/2011 and 19/05/2011) agree well – and are within error of – each other. (Table S2). The weighted mean date of R33 zircons analyzed during the first session was 415.9 ± 4.2 (2σ), with an MSWD of 2.3. The weighted mean of R33 zircons analyzed during the second session was 418.1 ± 4.4, with an MSWD of 2.2. These ages overlap within error with the accepted ID-TIMS age of 419.26 ± 0.39 reported by Black et al., (2004).

Trace element (P, Ti, Nd, Sm, Y, Zr, Th and Si) and REE (Ce, Eu, Dy and Lu) abundances were obtained simultaneously with the U and Pb isotopic measurements. Raw data were converted to concentrations (in ppm) by normalizing count rates for each element to those for Si, assuming SiO_2 to be stochiometric in zircon with a concentration of 32.8 wt%, and multiplying by a correction factor based on measurement of NIST 610 glass standard with

concentrations recommended by Pearce et al., (1997). The low abundance ^{49}Ti was chosen to avoid interference with ^{96}Zr and/or ^{48}Ca (from apatite inclusions) on the major ^{48}Ti peak. Values for Pr, Nd, Gd, Tb, Dy, Ho, Er and Tm were calculated through interpolation using equations stated in Bolhar et al., (2008). Unusually high P (>1500 ppm) and light rare earth element (LREE) count rates were interpreted to represent analysis of apatite inclusions, and where encountered, were excluded from age and concentration calculations. Following LA-ICPMS U-Pb analyses, estimates of crystallization age were made using the following criteria; A) exclusion of analyses that were >10% discordant and/or spot MSWDs >10, B) exclusion of analyses that indicate apatite inclusions (La >3 ppm; P >1500 ppm), C) crystallization age identified from inherited age population(s) on the basis of application of the mixture modeling procedure of Sambridge and Compston (1994), D) separate zircon age populations were identified where dates differ outside uncertainty.

High-Precision U-Pb Zircon Geochronology (ID-TIMS)

Four samples (P80361, P52235, P51290, P45972) were analyzed by the U-Pb ID-TIMS technique in the Isotope Laboratory at the Massachusetts Institute of Technology (MIT) using procedures outlined in Ramezani et al., (2011). All analyses were hand-selected single zircon grains pre-treated by the chemical abrasion technique (CA-TIMS of Mattinson, 2005) to mitigate the effects of radiation-induced Pb loss. A subset of zircon grains from sample P80361 were mechanically abraded using the air abrasion technique of Krogh (1982) prior to CA-TIMS treatment in order to explore the possibility of rim overgrowth on older zircon. In contrast to that in the LA-ICPMS analyses, zircon selection for ID-TIMS analyses were aimed at isolating the youngest population of grains that would best represent the age of pluton emplacement. This selection was based entirely on zircon morphology and clarity. The pre-treated zircons were spiked with the EARTHTIME mixed ^{205}Pb - ^{233}U - ^{235}U tracer prior to total dissolution and chemical separation of U and Pb. All isotopic measurements were made on the Sector54 multi-collector, thermal-ionization mass spectrometer at MIT. Data reduction, as well as date and error calculation follows the algorithm of McLean et al., (2011) and the EARTHTIME software applications (Bowring et al., 2011). All calculated ages (Table 3) are reported with 95% confidence uncertainty and include U-Pb tracer calibration errors.

S2. DATA REDUCTION METHODOLOGY FOR LA-ICPMS

Determining what, if any, geological factor(s) is responsible for the observed excess scatter in the presented zircon U-Pb LA-ICPMS data is not straightforward. There are several reasons that can explain a large scatter in any data set, including, but not limited to, mixed age domains within an individual spot analysis, multiple zircon age populations within a sample, and open system behavior in zircon, i.e., zircon inheritance or post-crystallization Pb loss. Due to the large spot size (~32μm) of the laser beam (relative to rim widths), delineation of the age and trace element composition of individual oscillatory zones within a single zircon grain was proven impossible; however, analyses of uninterrupted oscillatory-zoned bands are likely to reflect the average composition and conditions of the magma at the time of crystal growth and these were therefore specifically targeted to constrain the magmatic age. Inherited cores and whole zircons

interpreted to have been sourced from the Ordovician Greenland Group metasediments through which the suite of dated granites intrude are readily distinguishable on the basis of CL imaging (Fig. 3) and age populations that match detrital zircon age spectra within the Greenland Group. Young outliers within an analyzed sample are interpreted to represent Pb loss and were excluded from date calculations. Recognition of widespread Pb loss affecting the majority of zircon grains within a single sample was more difficult to identify and justify. In most cases, the geological setting (i.e., proximity to younger Cretaceous plutons), and excess scatter in dates with no clearly defined age population(s) provided the best evidence for widespread Pb-loss within individual samples.

A further complication in the interpretation of U-Pb dates obtained by LA-ICPMS is the likelihood of sampling multiple growth zones within a single analysis, including older inherited cores. Many of the samples analyzed in this study record complex histories of crustal inheritance and multiple episodes of magmatic crystallization. It is clear from Figure S5 that multiple domains representing different growth episodes may be sampled within an individual spot analysis. Figure S5 shows two examples of zircon grains from sample P51290 (Whakapoai) which display increasing ages with elapsed time/depth of ablation. Zircon grains from Whakapoai (P51290) appear to have magmatic overgrowths on slightly older premagmatic zircons which have survived the melting event, pluton emplacement and solidification processes. There are no obvious chemical or morphological differences between the magmatic and premagmatic zircons. As the laser drills deeper into the zircon grain, it is progressively sampling older zircon growth zones, and therefore 'mixed' ages between the interpreted magmatic age of 370.6 ± 3.0 Ma and the inherited premagmatic age of 386.2 ± 4.7 Ma are obtained. This pattern of two age populations and a spread of 'mixed ages' is also evident in sample P52283. Mixed ages are less evident in sample P31272, which are the two samples that lack a resolvable two-component age population. LA-ICPMS U-Pb dating of these complex zircons is not as robust a technique as SHRIMP U-Pb analysis which provides greater depth control, and is therefore less likely to drill into older inherited growth zones. For LA-ICPMS dating the result is a 'mixed' age between the interpreted magmatic age and the inherited age (i.e., Sagar and Palin, 2011). Trace element and U-Pb depth profile monitoring for each individual spot was undertaken to identify and eliminate analyses that represent drilling from younger into older zircon domains. As stated in the Discussion section, comparison of sample P51290 which was analyzed by both ID-TIMS and LA-ICPMS techniques reveals that the youngest dates obtained by LA-ICPMS are generally closest to the emplacement age determined by ID-TIMS; i.e., no significant Pb-loss has been detected in most cases.

Turnbull, R., Tulloch, A., Ramezani, J., and Jongens, R., 2016, Extension-facilitated pulsed S-I-A-type "flare-up" magmatism at 370 Ma along the southeast Gondwana margin in New Zealand: Insights from U-Pb geochronology and geochemistry: GSA Bulletin, doi:10.1130/B31426.1.

REFERENCES CITED

Ballard, J.R., Palin, J.M., Williams, I.S., Campbell, I.H., and Faunes, A., 2001, Two ages of porphyry intrusion resolved for the super-giant Chuquicamata copper deposit of northern Chile by ELA-ICP-MS and SHRIMP: Geology, v. 29, p. 383–386, doi:10.1130/0091-7613(2001)029<0383:TAOPIR>2.0.CO;2.

Black, L.P., Kamo, S.L., Allen, C.M., Davis, D.W., Aleinikoff, J.N., Valley, J.W., Mundil, R., Campbell, I.H., Korscha, R.J., Williams, I.S., and Foudoulis, C., 2004, Improved $^{206}Pb/^{238}U$ microprobe geochronology by the monitoring of a trace-element-related matrix effect; SHRIMP, ID–TIMS, ELA–ICP–MS and oxygen isotope documentation for a series of zircon standards: Chemical Geology, v. 205, p. 115–140, doi:10.1016/j.chemgeo.2004.01.003.

Bolhar, R., Weaver, S., Palin, J., Cole, J., and Paterson, L., 2008, Systematics of zircon crystallisation in the Cretaceous Separation Point Suite, New Zealand, using U-Pb isotopes, REE and Ti geothermometry: Contributions to Mineralogy and Petrology, v. 156, p. 133–160, doi:10.1007/s00410-007-0278-5.

Bowring, J.F., McLean, N.M., and Bowring, S.A., 2011, Engineering cyber infrastructure for U-Pb geochronology: Tripoli and U-Pb_Redux: Geochemistry Geophysics Geosystems, v. 12, doi:10.1029/2010GC003479.

Krogh, T.E., 1982, Improved accuracy of U-Pb zircon ages by the creation of more concordant systems using an air abrasion technique: Geochimica et Cosmochimica Acta, v. 46, p. 637–649, doi:10.1016/0016-7037(82)90165-X.

Mattinson, J.M., 2005, Zircon U/Pb chemical abrasion (CA-TIMS) method; combined annealing and multi-step partial dissolution analysis for improved precision and accuracy of zircon ages: Chemical Geology, v. 220, p. 47–66, doi:10.1016/j.chemgeo.2005.03.011.

McLean, N.M., Bowring, J.F., and Bowring, S.A., 2011, An algorithm for U-Pb isotope dilution data reduction and uncertainty propagation: Geochemistry Geophysics Geosystems, v. 12, doi:10.1029/2010GC003478.

Pearce, N.J.G., Perkins, W.T., Westgate, J.A., Gorton, M.P., Jackson, S.E., Neal, C.R., and Chenery, S.P., 1997, A compilation of new and published major and trace element data for NIST SRM 610 and NIST SRM 612 glass reference materials: Geostandards Newsletter, v. 21, p. 115–144, doi:10.1111/j.1751-908X.1997.tb00538.x.

Ramezani, J., Hoke, G.D., Fastovsky, D.E., Bowring, S.A., Therrien, F., Dworkin, S.I., Atchley, S.C., and Nordt, L.C., 2011, High-precision U-Pb zircon geochronology of the Late Triassic Chinle Formation, Petrified Forest National Park (Arizona, USA): Temporal constraints on the early evolution of dinosaurs: Geological Society of America Bulletin, v. 123, p. 2142–2159, doi:10.1130/B30433.1.

Sagar, M.W., and Palin, J.M., 2011, Emplacement, metamorphism, deformation and affiliation of mid-Cretaceous orthogneiss from the Paparoa Metamorphic Core Complex lower-plate, Charleston, New Zealand: New Zealand Journal of Geology and Geophysics, v. 54, p. 273–289, doi:10.1080/00288306.2011.562904.

Sambridge, M.S., and Compston, W., 1994, Mixture modeling of multi-component data sets with application to ion-probe zircon ages: Earth and Planetary Science Letters, v. 128, p. 373–390, doi:10.1016/0012-821X(94)90157-0.

Turnbull, R., Tulloch, A., Ramezani, J., and Jongens, R., 2016, Extension-facilitated pulsed S-I-A-type "flare-up" magmatism at 370 Ma along the southeast Gondwana margin in New Zealand: Insights from U-Pb geochronology and geochemistry: GSA Bulletin, doi:10.1130/B31426.1.

Figure S1. U-Pb concordia plot for single-grain ID-TIMS zircon analyses for Wangapeka (P80361). Single-grain ID-TIMS zircon analyses colored white (n = 3) represent air-abraded grains. Error ellipses and age uncertainties are both 2σ. The reported weighted mean ages include internal (analytical, spike calibration, and decay constant errors, as appropriate. MSWD – mean square of weighted deviates.

Figure S2. Th/U and Zr/Hf versus $T_{\text{Ti-in-zircon}}$ for Karamea Suite granites. Th/U ratios versus age for the Mt Radiant granite, and Kakapotahi granite.

Figure S3. Chondrite normalized REE diagrams for zircons from the Karamea Suite showing compositions for individual analyses. Analyses for each granite represent magmatic-aged zircons. Pooled individual analyses for inherited zircons at c. 387 Ma (A), c. 406 Ma (B = black lines), and c. 510–590 Ma (B = gray lines) are also shown for comparison.

Figure S4. Age versus $T_{\text{Ti-in-zircon}}$ for Karamea Suite granitoids. Grey lines show the calculated T_{Zr} for each of the samples based on whole-rock geochemistry. Black-filled symbols represent rim analyses, hollow symbols represent core/mid-section analyses.

Figure S5. Depth profile for two individual zircon spot analyses (spots #34 and #38) from the Whakapoai Granite (P51290) that reveal multiple growth zones with different ages with elapsed time/depth.

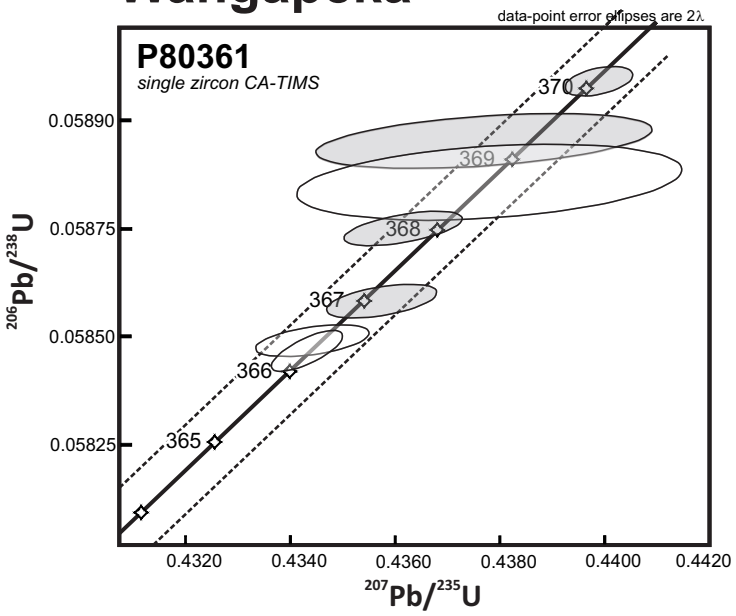
Wangapeka
data-point error ellipses are 2λ
P80361
single zircon CA-TIMS
370
369
368
367
366
365
0.05890
0.05875
0.05850
0.05825
206Pb/238U
0.4320
0.4340
0.4360
0.4380
0.4400
0.4420
207Pb/235U

FIG S1

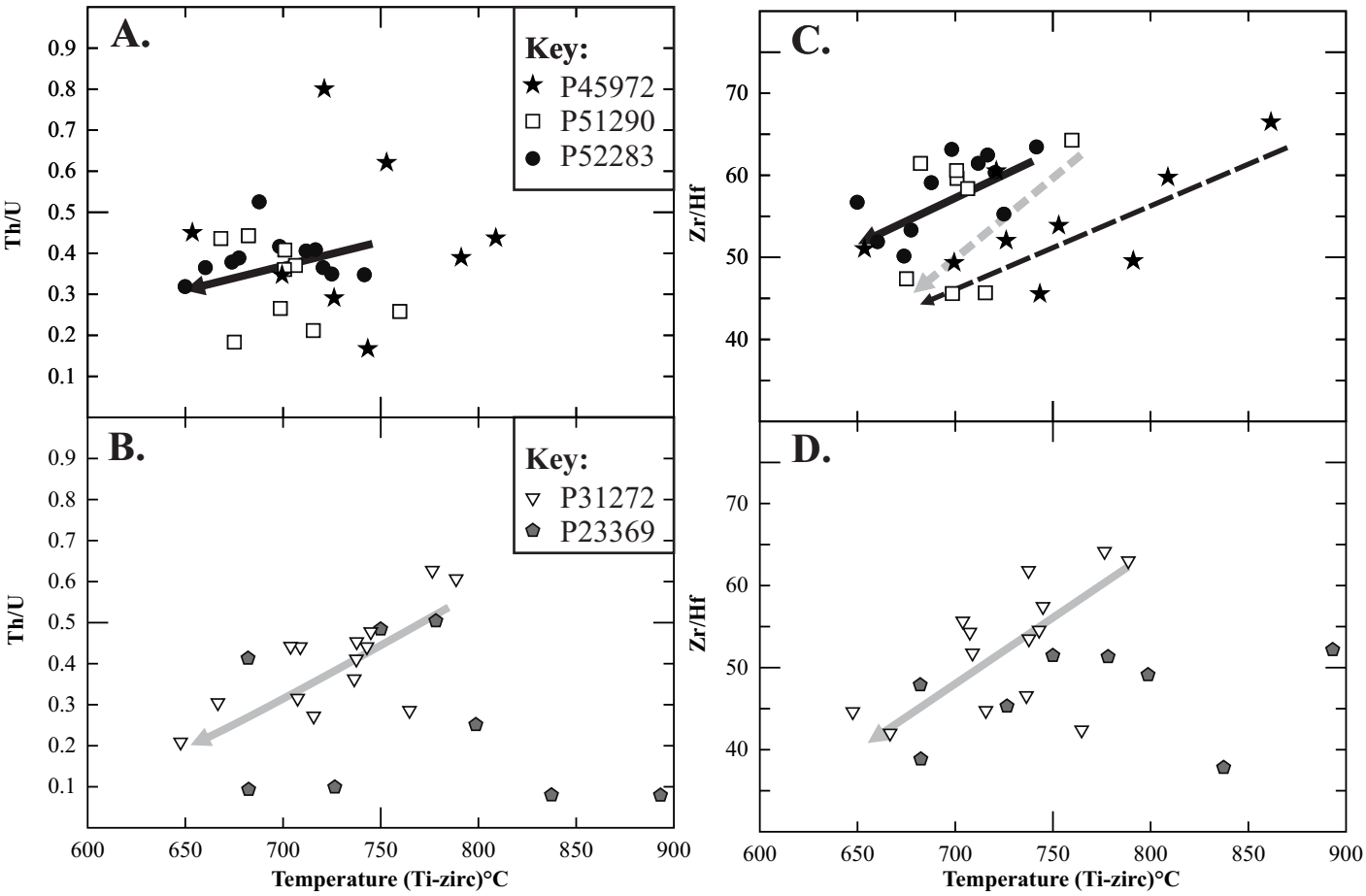
A.
Key:
P45972
P51290
P52283
B.
Key:
P31272
P23369
C.
D.
Th/U
Zr/Hf
Temperature (Ti-zirc)°C

FIG S2

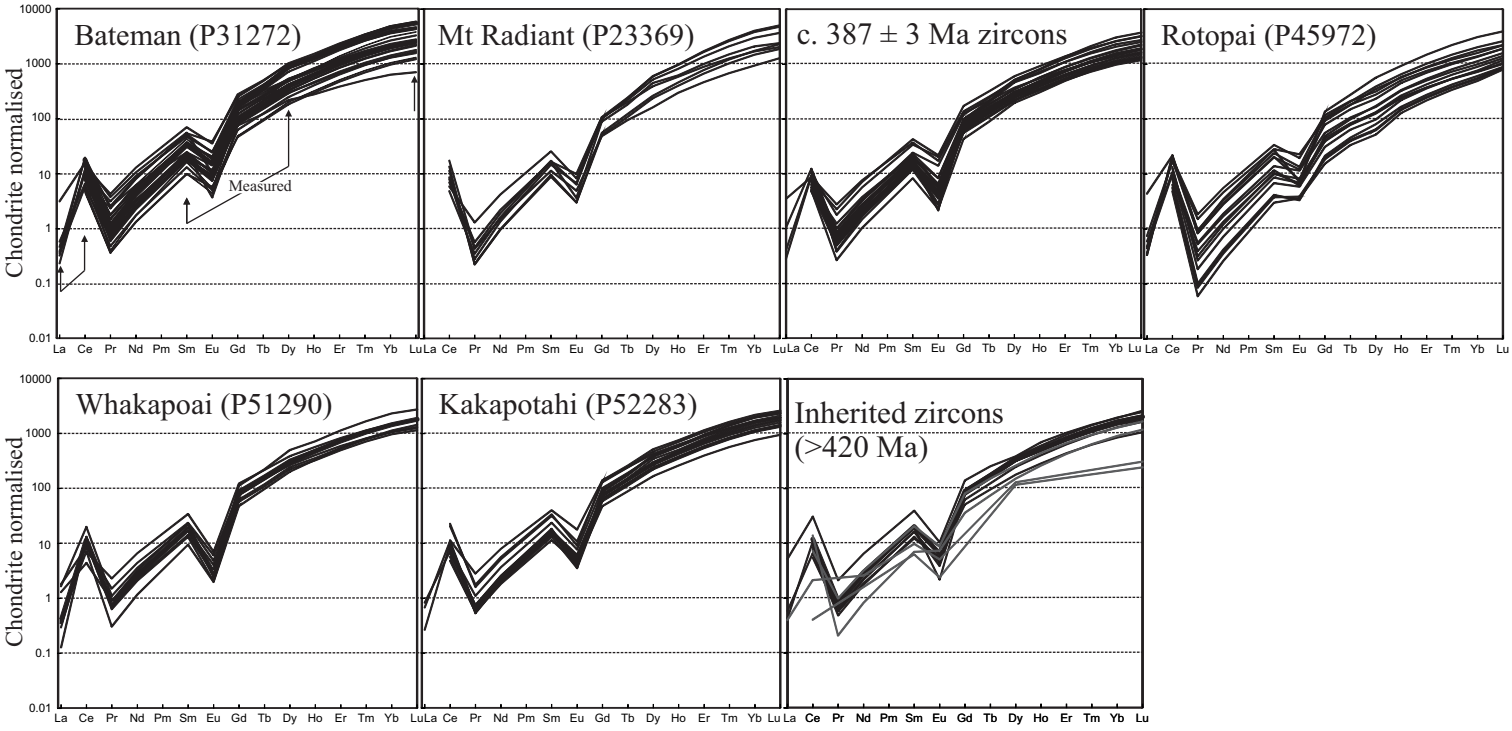
Bateman (P31272)
Mt Radiant (P23369)
c. 387 ± 3 Ma zircons
Rotopai (P45972)
Whakapoai (P51290)
Kakapotahi (P52283)
Inherited zircons
(>420 Ma)
Chondrite normalised
Measured
10000
1000
100
10
1
0.1
0.01
La Ce Pr Nd Pm Sm Eu Gd Tb Dy Ho Er Tm Yb Lu

FIG S3

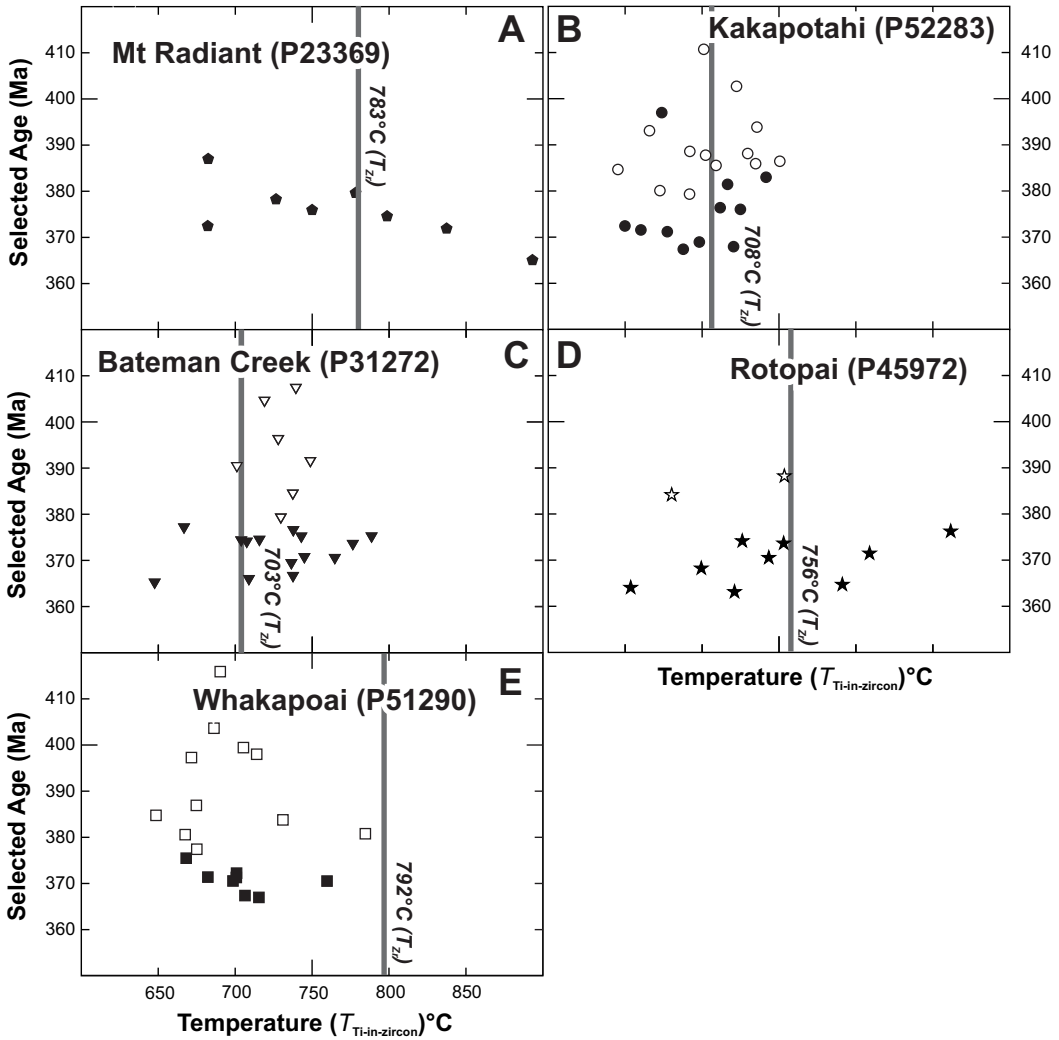
A
Mt Radiant (P23369)
783°C (T_{Zr})
B
Kakapotahi (P52283)
708°C (T_{Zr})
C
Bateman Creek (P31272)
703°C (T_{Zr})
D
Rotopai (P45972)
756°C (T_{Zr})
E
Whakapoai (P51290)
792°C (T_{Zr})
Selected Age (Ma)
360
370
380
390
400
410
650
700
750
800
850
Temperature ($T_{Ti\text{-}in\text{-}zircon}$)°C

FIG S4

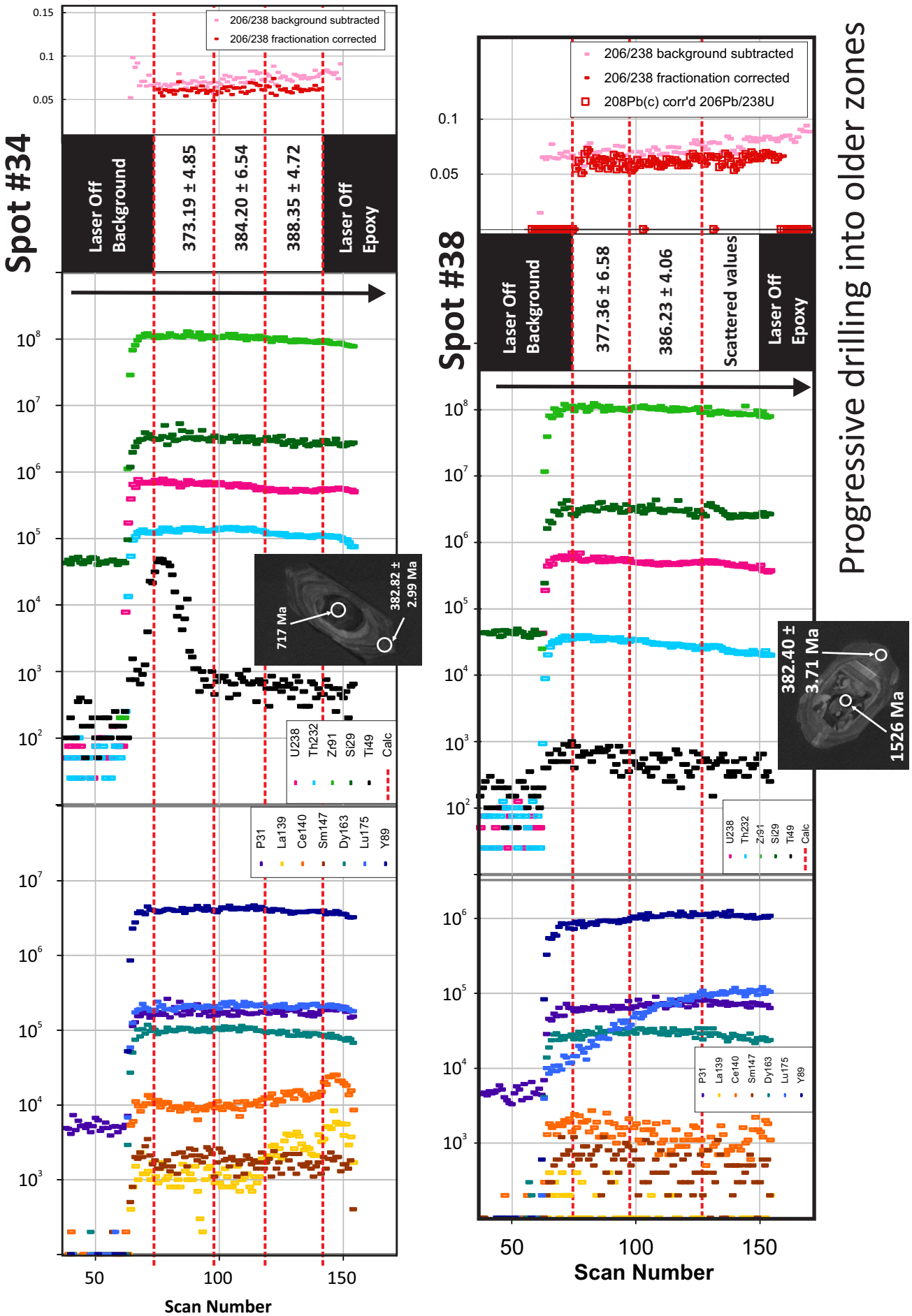
Spot #34
206/238 background subtracted
206/238 fractionation corrected
Laser Off Background
373.19 ± 4.85
384.20 ± 6.54
388.35 ± 4.72
Laser Off Epoxy
717 Ma
382.82 ± 2.99 Ma
U238
Th232
Zr91
Si29
Ti49
Calc
P31
La139
Ce140
Sm147
Dy163
Lu175
Y89
Scan Number
Spot #38
206/238 background subtracted
206/238 fractionation corrected
208Pb(c) corr'd 206Pb/238U
Laser Off Background
377.36 ± 6.58
386.23 ± 4.06
Scattered values
Laser Off Epoxy
382.40 ± 3.71 Ma
1526 Ma
Progressive drilling into older zones
Scan Number

FIG S5